Multibody Syst Dyn (2008) 20: 147–161
DOI 10.1007/s11044-008-9114-6

Implementation and efficiency of two geometric stiffening approaches

Urbano Lugrís · Miguel A. Naya · José A. Pérez · Javier Cuadrado

Received: 30 November 2007 / Accepted: 15 May 2008 / Published online: 23 July 2008

Abstract When the modeling of flexible bodies is required in multibody systems, the floating frame of reference formulations are probably the most efficient methods available. In the case of beams undergoing high speed rotations, the geometric stiffening effect can appear due to geometric nonlinearities, and it is often not captured by the aforementioned methods, since it is common to linearize the elastic forces assuming small deformations. The present work discusses the implementation of different existing methods developed to consider such geometric nonlinearities within a floating frame of reference formulation in natural coordinates, making emphasis on the relation between efficiency and accuracy of the resulting algorithms, seeking to provide practical criteria of use.

Keywords Flexibility · Efficiency · Geometric stiffening · Floating frame of reference

1 Introduction

One of the most widely used methods for flexible body modeling in multibody systems is the floating frame of reference approach (FFR) described by Shabana [1], in which a local frame of reference is attached to the flexible body, so that the elastic deformation is measured in the local frame and superimposed to the large amplitude motion, undergone by the reference frame. In most cases, component mode synthesis is used to approximate the deformation field, in order to improve the efficiency, thus restricting the application of these methods to small deformation problems. In specific applications, involving beams under high rotational speeds, such as helicopter rotor or turbine blades, the stiffening effect appears due to the geometrical nonlinearity. This effect has been studied by many authors, like Kane et al. [2], Mayo et al. [3, 4], Sharf [5], Shi et al. [6], or Valembois et al. [7]. Helicopter rotor blades, a typical example, are bent by their own weight, but the rotation speed makes them rise toward the horizontal position, due to centrifugal forces, as if the bending stiffness is increasing. In a linear model, this effect is not captured due to the absence of coupling between axial and

U. Lugrís (✉) · M.A. Naya · J.A. Pérez · J. Cuadrado
University of La Coruña, Ferrol, Spain
e-mail: ulugris@udc.es

transversal deformation, which implies that rotational speed has no effect on bending, but only on the radial displacement.

There exist several techniques aimed to include this effect in beams. In this paper, the implementation of two of them in a FFR formulation is described, and the results are compared to reference solutions obtained with fully nonlinear methods, such as the Absolute Nodal Coordinate Formulation (ANCF) proposed by Shabana [1] or the Finite Element Method (FEM) [8].

2 The specific FFR formulation

The equations of motion, according to an index-3 augmented Lagrangian formulation in natural dependent coordinates, García de Jalón and Bayo [9], Cuadrado et al. [10], are stated in the form,

$$\mathbf{M}\ddot{\mathbf{q}} + \mathbf{\Phi}_{\mathbf{q}}^T \alpha \mathbf{\Phi} + \mathbf{\Phi}_{\mathbf{q}}^T \boldsymbol{\lambda}^* = \mathbf{Q} \tag{1}$$

where $\mathbf{q}$ is the vector of natural coordinates, $\mathbf{M}$ is the mass matrix, $\mathbf{\Phi}$ and $\mathbf{\Phi}_{\mathbf{q}}$ are the constraints vector and its Jacobian matrix, α is the penalty factor, $\mathbf{Q}$ is the vector of elastic, applied and velocity-dependent inertia forces, and $\boldsymbol{\lambda}^*$ is the Lagrange multipliers vector, obtained from an iterative process carried out within each time-step,

$$\boldsymbol{\lambda}_{i+1}^* = \boldsymbol{\lambda}_i^* + \alpha \mathbf{\Phi}_{i+1} \quad i = 0, 1, 2, \ldots \tag{2}$$

which starts with $\boldsymbol{\lambda}_0^*$ equal to the value of $\boldsymbol{\lambda}^*$ obtained in the previous time-step. In the first time-step, $\boldsymbol{\lambda}_0^*$ can be initialized to zero. These equations are integrated in time by means of a Newmark-type integrator [11] (the trapezoidal rule), along with velocity and acceleration projections at the end of each time-step to preserve stability, Cuadrado et al. [10].

The case of a planar flexible beam is to be described for the sake of simplicity. However, the procedure can be generalized to the 3D case. The considered FFR approach defines the deformation of a flexible planar beam in a local reference frame, which is attached to a material point of the beam and undergoes the large amplitude rigid-body motion. The position $\mathbf{r}$ of any point of the solid can be expressed as

$$\mathbf{r} = \mathbf{r}_0 + \mathbf{A}\,(\bar{\mathbf{r}}_{\mathrm{u}} + \delta\bar{\mathbf{r}}) \tag{3}$$

where $\mathbf{r}_0$ is the position of the local frame origin, $\mathbf{A}$ the rotation matrix defined by the two orthogonal local unit vectors $[\mathbf{u}|\mathbf{v}]$, $\bar{\mathbf{r}}_{\mathrm{u}}$ the undeformed position in local coordinates, and $\delta\bar{\mathbf{r}}$ the local elastic displacement (see Fig. 1).

Using the finite element method to discretize the beam with 2D beam elements, the neutral axis displacement within a finite element e, $\delta\bar{\mathbf{r}}_0^e$, can be interpolated from its nodal displacements, $\mathbf{q}_{\mathrm{f}}^e$, by means of the interpolation matrix, $\mathbf{S}^e$, which can be split into longitudinal and transversal interpolation submatrices, $\mathbf{S}_{\mathrm{l}}^e$ and $\mathbf{S}_{\mathrm{t}}^e$,

$$\delta\bar{\mathbf{r}}_0^e = \begin{Bmatrix} u_0 \\ v_0 \end{Bmatrix} = \mathbf{S}^e \mathbf{q}_{\mathrm{f}}^e = \begin{bmatrix} \mathbf{S}_{\mathrm{l}}^e \\ \mathbf{S}_{\mathrm{t}}^e \end{bmatrix} \mathbf{q}_{\mathrm{f}}^e \tag{4}$$

where u_0 and v_0 are the local components of $\delta\bar{\mathbf{r}}_0^e$.

The dimension of the finite element model is reduced by using component mode synthesis, in this case, a Craig–Bampton reduction, Craig and Bampton [12], with static and

Fig. 1 Deformed 2D beam

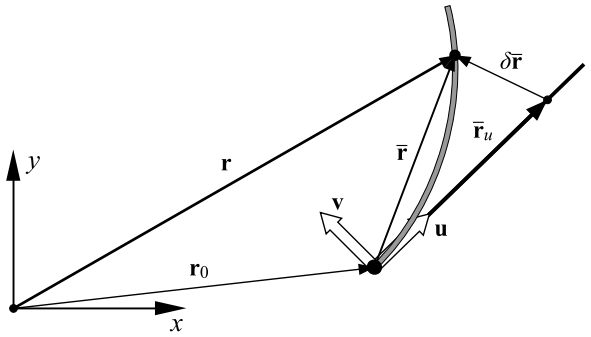

dynamic modes, as done by Cuadrado et al. [10]. This reduction consists of approximating the vector of nodal displacements by means of a linear combination of *ns* static modes $\mathbf{\Phi}_i$ and *nd* dynamic modes $\mathbf{\Psi}_j$,

$$\mathbf{q}_\mathrm{f} = \sum_{i=1}^{ns} \mathbf{\Phi}_i \eta_i + \sum_{j=1}^{nd} \mathbf{\Psi}_j \xi_j \tag{5}$$

where $\mathbf{q}_\mathrm{f}$ is a vector grouping all the nodal displacements of the beam, and the coefficients η_i and ξ_j are the modal amplitudes. The static modal amplitudes must be bound to the natural coordinates of the corresponding joints through kinematic constraints. Equation (5) can be written in a more compact matrix form,

$$\mathbf{q}_\mathrm{f} = \begin{bmatrix} \mathbf{\Phi}_1 & \cdots & \mathbf{\Phi}_{ns} & \mathbf{\Psi}_1 & \cdots & \mathbf{\Psi}_{nd} \end{bmatrix} \begin{Bmatrix} \eta_1 \\ \vdots \\ \eta_{ns} \\ \xi_1 \\ \vdots \\ \xi_{nd} \end{Bmatrix} = \mathbf{X}\mathbf{y} \tag{6}$$

Finally, the vector of variables for a single flexible beam results,

$$\mathbf{q}^T = \begin{Bmatrix} \mathbf{r}_0^T & \mathbf{u}^T & \mathbf{v}^T & \eta_1 & \cdots & \eta_{ns} & \xi_1 & \cdots & \xi_{nd} \end{Bmatrix} = \begin{Bmatrix} \mathbf{r}_0^T & \mathbf{u}^T & \mathbf{v}^T & \mathbf{y}^T \end{Bmatrix} \tag{7}$$

With all the flexible body kinematics defined, the mass matrix can be calculated. The elastic displacement can be specified for node i as $\delta\bar{\mathbf{r}}_0^i = \mathbf{q}_\mathrm{f}^i = \mathbf{X}^i\mathbf{y}$, being $\mathbf{X}^i$ the couple of rows of $\mathbf{X}$ corresponding to the longitudinal and transversal displacements of node i. The absolute velocity of node i, $\mathbf{v}^i$, can be calculated by substituting its elastic displacement in (3), and differentiating with respect to time,

$$\mathbf{v}^i = \dot{\mathbf{r}}_0 + \dot{\mathbf{A}}\left(\bar{\mathbf{r}}_0^i + \mathbf{X}^i\mathbf{y}\right) + \mathbf{A}\mathbf{X}^i\dot{\mathbf{y}} \tag{8}$$

At this point, the corotational approach proposed by Géradin and Cardona [13] is adopted in order to simplify the mass matrix calculation, Cuadrado et al. [10]. Although it is not fully consistent with the FFR formalism, the finite element displacement interpolation matrices $\mathbf{S}^e$ are used to interpolate nodal velocities, an approximation that becomes exact when the

element size tends to zero. Accordingly, the kinetic energy can be written in terms of the nodal velocities $\mathbf{v}$ and the finite element mass matrix $\mathbf{M}_{\text{fe}}$,

$$T = \frac{1}{2}\int_V \dot{\mathbf{r}}^T \dot{\mathbf{r}}\, \mathrm{d}m = \frac{1}{2}\int_V \mathbf{v}^T \mathbf{S}^T \mathbf{S}\mathbf{v}\, \mathrm{d}m = \frac{1}{2}\mathbf{v}^T \mathbf{M}_{\text{fe}}\mathbf{v} \tag{9}$$

where $\mathbf{S}$ contains the assembled interpolation matrices of all the finite elements of the flexible body. Equation (8) can be written in matrix form for all the nodes, since it is linear with respect to the generalized velocities $\dot{\mathbf{q}}$,

$$\mathbf{v} = \mathbf{B}(\mathbf{q})\,\dot{\mathbf{q}} \tag{10}$$

Finally, this relationship can be substituted into (9) to obtain the mass matrix,

$$\mathbf{M} = \mathbf{B}^T \mathbf{M}_{\text{fe}} \mathbf{B} \tag{11}$$

The velocity-dependent inertia forces vector $\mathbf{Q}_{\text{v}} = -\mathbf{B}^T \mathbf{M}_{\text{fe}} \dot{\mathbf{B}}\dot{\mathbf{q}}$ must be added to the generalized forces vector $\mathbf{Q}$. The calculation of the elastic forces will be addressed in the following section.

3 Geometric nonlinearity consideration

The elastic displacements field $\delta\bar{\mathbf{r}}(x, y)$ of an Euler–Bernoulli beam takes the following vector form, Sharf [5],

$$\delta\bar{\mathbf{r}}(x, y) = \begin{Bmatrix} u \\ v \end{Bmatrix} = \begin{Bmatrix} u_0 - y v_0' \\ v_0 \end{Bmatrix} \tag{12}$$

where u_0 and v_0 are the axial and transversal displacements of the neutral axis, and the apostrophe indicates differentiation with respect to the x coordinate. The nonlinear strain-displacement relationship in x direction can be expressed as

$$\varepsilon_{xx} = u' + \frac{1}{2}\left(u'^2 + v'^2\right) \cong u' + \frac{1}{2}v'^2 \tag{13}$$

where the term u'^2 is dropped since it is much smaller than u'. The elastic potential of the beam, after applying the stress-strain relation is

$$U = \frac{1}{2}\int_V E\varepsilon_{xx}^2\, \mathrm{d}V \tag{14}$$

where E is the Young modulus and V is the volume of the beam. Introduction of the displacement field described by (12) in the strain-displacement relation, yields the deformation energy of the beam in terms of the neutral axis deformed shape [5],

$$U = \underbrace{\frac{1}{2}\int_0^L EAu_0'^2\, \mathrm{d}x + \frac{1}{2}\int_0^L EIv_0''^2\, \mathrm{d}x}_{\textit{Linear formulation}} + \underbrace{\frac{1}{2}\int_0^L EAu_0'v_0'^2\, \mathrm{d}x}_{\textit{First nonlinear}} + \underbrace{\frac{1}{8}\int_0^L EAv_0'^4\, \mathrm{d}x}_{\textit{Second nonlinear}} \tag{15}$$

with A the cross-sectional area and I the second moment of area with respect to the neutral axis.

Different levels of approximation can be achieved depending on which terms of (15) are kept: They are discussed in the following subsections.

3.1 Linear formulation

The linear formulation includes only the first two terms of (15) in the elastic potential, neglecting the higher order ones. Introducing the finite element discretization into the equation and integrating the interpolation functions, the following expression can be obtained for the elastic potential in terms of the finite element coordinates,

$$U = \frac{1}{2}\mathbf{q}_{\mathrm{f}}^{T}\mathbf{K}_{\mathrm{L}}^{\mathrm{fe}}\mathbf{q}_{\mathrm{f}} \tag{16}$$

Here, $\mathbf{K}_{\mathrm{L}}^{\mathrm{fe}}$ is the linear stiffness matrix, which is constant, and $\mathbf{q}_{\mathrm{f}}$ is a vector containing the nodal displacements of the whole beam. This potential can be projected into the modal base by using matrix $\mathbf{X}$,

$$U = \frac{1}{2}\mathbf{y}^{T}\mathbf{X}^{T}\mathbf{K}_{\mathrm{L}}^{\mathrm{fe}}\mathbf{X}\mathbf{y} = \frac{1}{2}\mathbf{y}^{T}\mathbf{K}_{\mathrm{L}}\mathbf{y} \tag{17}$$

By differentiation of the elastic potential, an expression for the elastic forces is obtained,

$$\mathbf{F}_{\mathrm{el}} = -\left(\frac{\partial U}{\partial \mathbf{y}}\right)^{T} = -\mathbf{K}_{\mathrm{L}}\mathbf{y} \tag{18}$$

which is a linear relationship between the forces and the modal amplitudes.

A closer look to the elastic potential expression used in this formulation, constituted by the first two terms of (15), reveals the cause of its inability to capture the geometric stiffening effect: axial and transversal displacements separately contribute to the deformation energy. Only transversal forces can produce transversal displacements, therefore, the axial forces introduced by the rotation have no effect on the deflection.

3.2 First nonlinear formulation

When the third term of (15) is considered also, the coupling between axial and transversal deformation is introduced through the integral of $u_0' v_0'^{2}$. This allows us to capture the geometric stiffening effect, since it couples the longitudinal and the transversal displacements, but at the cost of a nonconstant stiffness matrix.

The same steps as in the linear formulation must be carried out to obtain the elastic potential: the u_0 and v_0 derivatives are substituted by their finite element interpolations, and the integrals are evaluated; then writing it in matrix form, Mayo et al. [3, 4],

$$U = \frac{1}{2}\mathbf{q}_{\mathrm{f}}^{T}\left(\mathbf{K}_{\mathrm{L}}^{\mathrm{fe}} + \mathbf{K}_{\mathrm{G}}^{\mathrm{fe}}\right)\mathbf{q}_{\mathrm{f}} \tag{19}$$

The geometric stiffness matrix $\mathbf{K}_{\mathrm{G}}^{\mathrm{fe}}$ is variable, and must be calculated at every time-step. In case that the axial displacement u_0 has a linear distribution, the strain is constant along the whole beam, and $\mathbf{K}_{\mathrm{G}}^{\mathrm{fe}}$ can be expressed as the product of a scalar variable times a constant matrix. But in any other case, this is only applicable to each finite element, and the matrix must be assembled at every time-step, which is rather inefficient.

It is better to express u_0 and v_0 in terms of the mode shapes and then carry out the spatial integration. First, the neutral axis displacements are approximated by the modal superposition,

$$\begin{aligned} u_0(x) &= \sum_{i=1}^{ns} \phi_i^{\mathrm{l}}(x)\eta_i + \sum_{j=1}^{nd} \psi_j^{\mathrm{l}}(x)\xi_j \\ v_0(x) &= \sum_{i=1}^{ns} \phi_i^{\mathrm{t}}(x)\eta_i + \sum_{j=1}^{nd} \psi_j^{\mathrm{t}}(x)\xi_j \end{aligned} \tag{20}$$

where the superindices l and t indicate longitudinal or transversal component, respectively. These approximated displacements are then used to calculate the integral. The analytical functions of the mode shapes are usually known for a beam and, therefore, they can be directly integrated. In the case that the modes are finite element displacement vectors, the integrals must be calculated by using the interpolation functions. The geometric stiffness matrix, already projected into the modal subspace, takes the following linear combination form, with the modal amplitudes as coefficients,

$$\mathbf{K}_{\mathrm{G}} = \sum_{i=1}^{ns} \eta_i \mathbf{K}_{\mathrm{G}i} + \sum_{j=1}^{nd} \xi_j \mathbf{K}_{\mathrm{G}j} \tag{21}$$

where all the $\mathbf{K}_{\mathrm{G}i}$ and $\mathbf{K}_{\mathrm{G}j}$ matrices are constant, and have the form,

$$\mathbf{K}_{\mathrm{G}i} = \int_0^L EA\phi_i'^{\mathrm{l}} \begin{Bmatrix} \phi_1'^{\mathrm{t}} \\ \vdots \\ \phi_{ns}'^{\mathrm{t}} \\ \psi_1'^{t} \\ \vdots \\ \psi_{nd}'^{\mathrm{t}} \end{Bmatrix} \begin{Bmatrix} \phi_1'^{\mathrm{t}} & \cdots & \phi_{ns}'^{\mathrm{t}} & \psi_1'^{\mathrm{t}} & \cdots & \psi_{nd}'^{\mathrm{t}} \end{Bmatrix} \mathrm{d}x \tag{22}$$

with $\psi_j'^{\mathrm{l}}$ instead of $\phi_i'^{\mathrm{l}}$ for $\mathbf{K}_{\mathrm{G}j}$. These matrices are nonzero for mode i or j only if the mode is longitudinal, so that there is one matrix for each axial mode. According to this, in order to obtain a nonzero $\mathbf{K}_{\mathrm{G}}$ matrix, this method needs to incorporate at least one axial mode.

Differentiation of the elastic potential with respect to $\mathbf{y}$, neglecting the term which contains the derivative of $\mathbf{K}_{\mathrm{G}}$, yields the elastic forces vector,

$$\mathbf{F}_{\mathrm{el}} = -\left(\frac{\partial U}{\partial \mathbf{y}}\right)^T = -\left(\mathbf{K}_{\mathrm{L}} + \mathbf{K}_{\mathrm{G}}\right)\mathbf{y} \tag{23}$$

The modifications with respect to the linear formulation are minimal. All the integrals of (22) must be calculated in a preprocessing stage, thus obtaining one constant matrix for each axial mode. Since the stiffness matrix is no longer constant, it must be calculated at every integrator iteration by adding the variable $\mathbf{K}_{\mathrm{G}}$ to the linear stiffness matrix $\mathbf{K}_{\mathrm{L}}$.

3.3 Second nonlinear formulation

In this formulation, the four terms of the elastic energy in (15) are considered, being the most suitable for severe deformation conditions but logically at the cost of a higher computational

effort

$$U = \frac{1}{2}\mathbf{q}_{\mathrm{f}}^{T}\left(\mathbf{K}_{\mathrm{L}}^{\mathrm{fe}} + \mathbf{K}_{\mathrm{G}}^{\mathrm{fe}} + \mathbf{K}_{\mathrm{H}}^{\mathrm{fe}}\right)\mathbf{q}_{\mathrm{f}} \tag{24}$$

The inclusion of the higher order term adds a second-order nonlinear matrix $\mathbf{K}_{\mathrm{H}}^{\mathrm{fe}}$, and the elastic forces are obtained by differentiation,

$$\mathbf{F}_{\mathrm{el}} = -\left(\frac{\partial U}{\partial \mathbf{q}_{\mathrm{f}}}\right)^{T} = -\left(\mathbf{K}_{\mathrm{L}}^{\mathrm{fe}} + \mathbf{K}_{\mathrm{G}}^{\mathrm{fe}} + \mathbf{K}_{\mathrm{H}}^{\mathrm{fe}}\right)\mathbf{q}_{\mathrm{f}} + \mathbf{Q}_{\mathrm{g}} \tag{25}$$

where all the terms depending on the derivatives of the nonconstant $\mathbf{K}$ matrices are grouped into the generalized nonlinear forces vector $\mathbf{Q}_{\mathrm{g}}$. The main problem of this formulation is that it needs a high number of axial modes to obtain accurate results, Mayo et al. [3, 4], making its use inefficient.

3.4 Foreshortening formulation

The axial shortening of a beam due to its deflection is known as foreshortening (Fig. 2). This effect cannot be captured by using the linear or first nonlinear formulations. The explicit inclusion of the foreshortening effect in the model leads to a simpler and more efficient method, Mayo et al. [3, 4], and provides the same level of accuracy as the second nonlinear formulation.

The longitudinal displacement of any point at the neutral axis can be divided into the axial deformation produced by the actual axial forces, s, and the shortening produced by the deflection u_{fs},

$$u_0 = s + u_{fs} \tag{26}$$

The foreshortening of a curve infinitesimal ds can be obtained, as shown in Fig. 3, from the projection of ds − dx into the undeformed neutral axis,

$$\mathrm{d}fs = (\mathrm{d}s - \mathrm{d}x)\cos\alpha = \left(1 - \frac{\mathrm{d}x}{\mathrm{d}s}\right)\mathrm{d}x = \left(1 - \frac{1}{\sqrt{1 + v_0'^{\,2}}}\right)\mathrm{d}x \tag{27}$$

This expression can be simplified for small values of v_0', by developing it into a Taylor series up to second order,

$$\mathrm{d}fs \approx \frac{1}{2}v_0'^{\,2}\,\mathrm{d}x \tag{28}$$

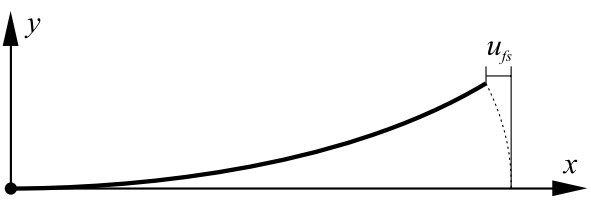

Fig. 2 Foreshortening produced by deflection

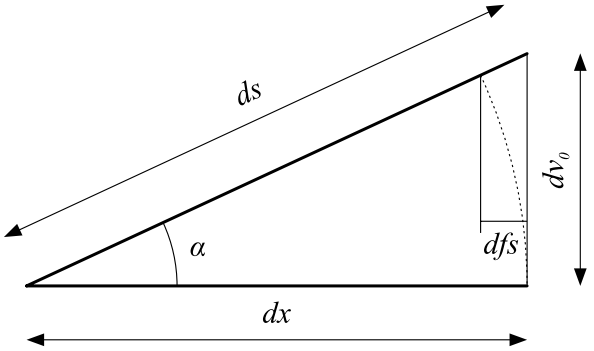

Fig. 3 Foreshortening of a curve infinitesimal

The total shortening accumulated from a reference point x_0, which has zero axial displacement is then obtained by integration,

$$u_{fs}(x) = -\frac{1}{2}\int_{x_0}^{x} v_0'^2 \, \mathrm{d}x \tag{29}$$

Substituting the longitudinal displacement of (26) into (15), yields the following expression for the elastic potential,

$$U = \frac{1}{2}\int_0^L EA s'^2 \, \mathrm{d}x + \frac{1}{2}\int_0^L EI v_0''^2 \, \mathrm{d}x \tag{30}$$

It is observed that the elastic energy has the same form as in the linear formulation, although the meaning is different. The stiffness matrix is the same as the one used for the linear case $\mathbf{K}_\mathrm{L}$, and so happens with the elastic forces. Therefore, the stiffening effect does not appear now in the elastic forces; it is translated to the inertia and constraint forces, since the foreshortening is introduced at kinematic level.

In order to calculate the total foreshortening on a finite element, the nodal displacement must be modified so that

$$\delta\bar{\mathbf{r}}_0^e = \begin{Bmatrix} u_0 \\ v_0 \end{Bmatrix} = \begin{bmatrix} \mathbf{S}_\mathrm{l}^e \\ \mathbf{S}_\mathrm{t}^e \end{bmatrix} \mathbf{q}_\mathrm{f}^e + \begin{Bmatrix} u_{fs}^e \\ 0 \end{Bmatrix} \tag{31}$$

where u_{fs}^e is the foreshortening produced in that finite element by its own deflection, and can be calculated by applying (29) over the whole length of the element, L^e. Substituting v_0' by its interpolation,

$$u_{fs}^e = -\frac{1}{2}\int_0^{L^e} \mathbf{q}_\mathrm{f}^{eT} \frac{\partial \mathbf{S}_\mathrm{t}^{eT}}{\partial x} \frac{\partial \mathbf{S}_\mathrm{t}^e}{\partial x} \mathbf{q}_\mathrm{f}^e \, \mathrm{d}x = -\frac{1}{2}\mathbf{q}_\mathrm{f}^{eT} \mathbf{H}^e \mathbf{q}_\mathrm{f}^e \tag{32}$$

The shortening suffered by one element is then a quadratic function of the nodal coordinates, where $\mathbf{H}^e$ is a constant matrix depending only on the transversal interpolation functions and the length of the element.

The total shortening accumulated by the finite elements located between the reference node (with zero axial displacement) and the finite element n, itself included, is the sum of

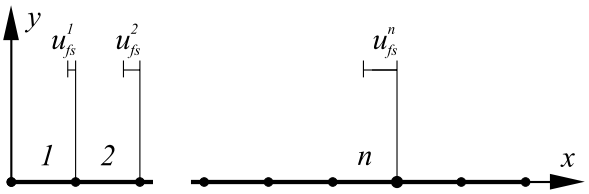

Fig. 4 Accumulated foreshortening at element n

all the element-level shortenings, as shown in Fig. 4

$$u_{fs}^n = -\frac{1}{2}\sum_{e=1}^{n} \mathbf{q}_{\mathrm{f}}^{eT}\mathbf{H}^e\mathbf{q}_{\mathrm{f}}^e \tag{33}$$

This expression can be written in matrix form for each element, assembled for all the finite element coordinates of the beam, and then projected into the modal subspace,

$$u_{fs}^n = -\frac{1}{2}\mathbf{q}_{\mathrm{f}}^T\mathbf{H}_{\mathrm{acc}}^n\mathbf{q}_{\mathrm{f}} = -\frac{1}{2}\mathbf{y}^T\mathbf{X}^T\mathbf{H}_{\mathrm{acc}}^n\mathbf{X}\mathbf{y} = -\frac{1}{2}\mathbf{y}^T\mathbf{G}^n\mathbf{y} \tag{34}$$

If analytical functions are available for the mode shapes, these $\mathbf{G}^n$ matrices can be directly calculated by using the second expression of (20) to evaluate (29),

$$\mathbf{G}^n = \int_0^{L^n} \begin{Bmatrix} \phi_1'^{\mathrm{t}} \\ \vdots \\ \phi_{ns}'^{\mathrm{t}} \\ \psi_1'^{\mathrm{t}} \\ \vdots \\ \psi_{nd}'^{\mathrm{t}} \end{Bmatrix} \begin{Bmatrix} \phi_1'^{\mathrm{t}} & \cdots & \phi_{ns}'^{\mathrm{t}} & \psi_1'^{\mathrm{t}} & \cdots & \psi_{nd}'^{\mathrm{t}} \end{Bmatrix} \mathrm{d}x \tag{35}$$

where L^n is the length of the beam from the reference point to the end node (node i) of finite element n. If the modes are finite element displacement vectors, the integrals must be calculated by using the interpolation functions.

Therefore, the elastic displacement of node i is now,

$$\delta\bar{\mathbf{r}}_0^i = \mathbf{q}_{\mathrm{f}}^i + \begin{Bmatrix} u_{fs}^n \\ 0 \end{Bmatrix} = \mathbf{X}^i\mathbf{y} + \begin{Bmatrix} u_{fs}^n \\ 0 \end{Bmatrix} = \mathbf{X}^i\mathbf{y} - \frac{1}{2}\begin{Bmatrix} 1 \\ 0 \end{Bmatrix}\mathbf{y}^T\mathbf{G}^n\mathbf{y} \tag{36}$$

Substituting this displacement into (3), and carrying out the time derivative results for the nodal velocity,

$$\mathbf{v}^i = \dot{\mathbf{r}}_0 + \dot{\mathbf{A}}\left(\bar{\mathbf{r}}_{\mathbf{u}}^i + \mathbf{X}_{fs}^i\right) + \mathbf{A}\left(\mathbf{X}_{fs}^i\dot{\mathbf{y}} + \dot{\mathbf{X}}_{fs}^i\mathbf{y}\right) \tag{37}$$

where $\mathbf{X}_{fs}$ is a variable matrix, which depends linearly on the modal amplitudes $\mathbf{y}$,

$$\mathbf{X}_{fs}^i = \mathbf{X}^i - \frac{1}{2}\begin{Bmatrix} 1 \\ 0 \end{Bmatrix}\mathbf{y}^T\mathbf{G}^i \tag{38}$$

In order to implement the foreshortening in the equations of motion, the $\mathbf{G}^n$ accumulated shortening matrices must be first calculated and stored in a preprocessing stage. Then the

new $\mathbf{X}_{fs}$ matrix, which is no longer constant, is calculated at every time-step and used to calculate matrix $\mathbf{B}$, as it was done in (8).

These changes affect the mass matrix, the velocity-dependent inertia forces and the applied forces. Moreover, those constraints involving nodes undergoing foreshortening must also be modified, since transversal modes affect the beam length. Therefore, the geometric stiffening effect is considered now through inertia and constraint forces, instead of through the elastic forces, as it happened in the first and second nonlinear formulations.

4 Examples and results

The example system is a typical case of geometric stiffening, Kane et al. [2], Mayo et al. [3, 4], Sharf [5], Shi et al. [6], Valembois et al. [7]: a beam pinned at one of its ends, as shown in Fig. 5, which rotates an angle $\theta(t)$ about the origin,

$$\theta(t) = \begin{cases} \frac{\omega_s}{T_s}\left(\frac{t^2}{2} + \left(\frac{T_s}{2\pi}\right)^2\left[\cos\left(\frac{2\pi t}{T_s}\right) - 1\right]\right) & 0 \le t < T_s \\ \omega_s\left(t - \frac{T_s}{2}\right) & T_s \le t \end{cases} \tag{39}$$

The characteristics of the beam are: length $L = 10$ m, cross-sectional area $A = 4 \cdot 10^{-4}$ m^2, second moments of area $I_{y,z} = 2 \cdot 10^{-7}$ m^4, density $\rho = 3000$ Kg/m^3 and Young modulus $E = 7 \cdot 10^{10}$ N/m^2.

4.1 Two-dimensional case

In [2–7], this example is treated as a 2D problem, studying the behavior of the beam in the xy plane in absence of gravity acceleration. The measured variable is the in-plane tip deflection, for $T_s = 15$ s and $\omega_s = 6$ rad/s.

A discretization into 10 finite elements is used, using one transversal static mode and two transversal dynamic modes. A reference solution has been calculated with a global, finite-element based formulation, the ANCF, Shabana [1], which uses absolute positions and slopes as coordinates in a global inertial reference frame. This formulation applies nonlinear strain-displacement relationships, so capturing all nonlinear effects, including geometric stiffening. In the simulation of reference the beam is discretized into 15 elements, using an ANCF-based 2D beam element developed by Omar and Shabana [14].

The results obtained for the linear formulation reveal that as expected, it cannot account for the geometric stiffening effect. As can be seen in Fig. 6, the tip deflection becomes too large, crashing the simulation before its end.

The first nonlinear formulation needs to include at least one axial mode, as the geometric stiffness matrix depends on the axial deformation. In the example, the axial displacement, caused by centrifugal forces, has a nonlinear distribution, so that the first dynamic axial

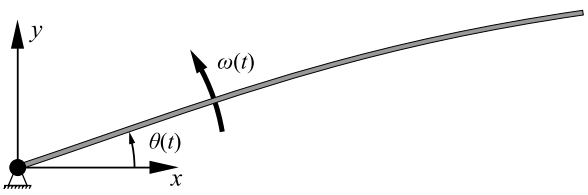

Fig. 5 Spin-up beam

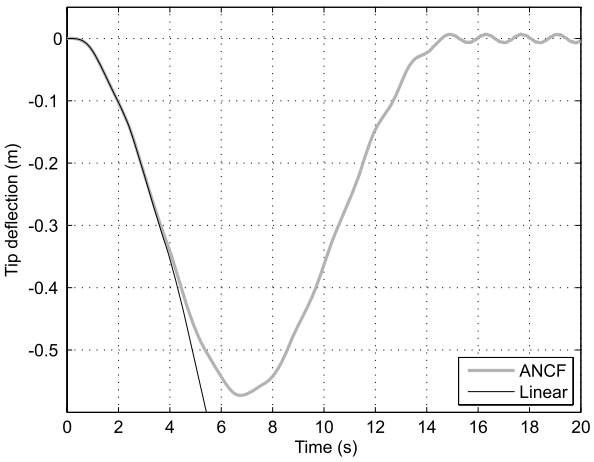

Fig. 6 Linear formulation vs. ANCF in the first example

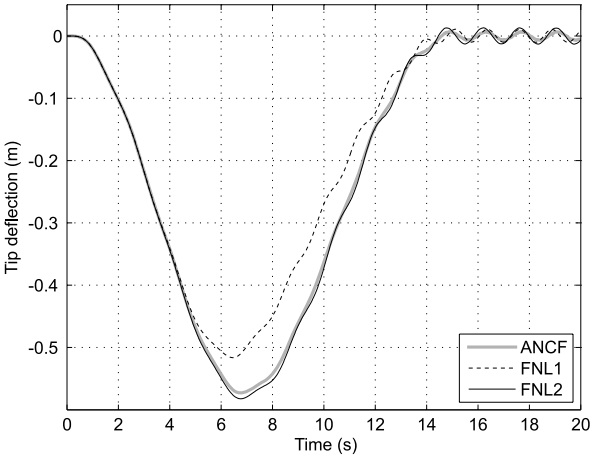

Fig. 7 First nonlinear formulation vs. ANCF in the first example

mode is required to achieve reasonable accuracy. Figure 7 shows that using only one linear static mode (FNL1 curve) yields unacceptable results, increasing the stiffness excessively. Therefore, two axial modes are needed at least to correctly simulate the motion of the beam (FNL2 curve).

The foreshortening formulation (FS curve in Fig. 8) achieves the best results, despite the absence of axial modes. The quality of the correlation becomes more obvious at the steady-state stage, where the first nonlinear formulation shows a higher oscillation amplitude.

Table 1 shows the CPU-times for all the simulations, run with the same integrator and parameters, with a time-step of 0.01 s. The formulations are sorted by accuracy, from lower to highest, according to the error measurement defined in (41): first nonlinear with one axial mode (FNL1), first nonlinear with two axial modes (FNL2), and foreshortening (FS0). The FS method is the fastest, due to the lower number of modes used, and to the absence of high frequency axial modes.

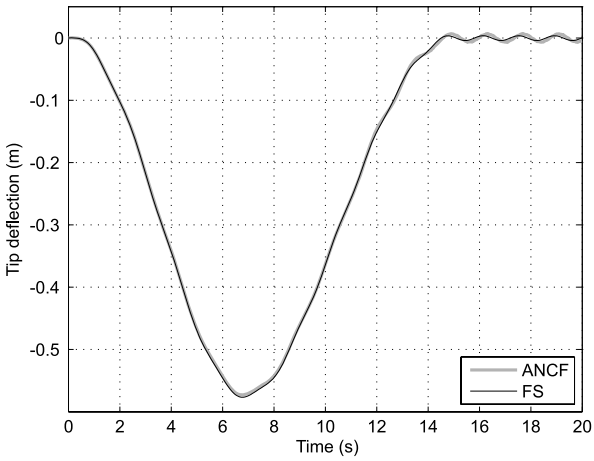

Fig. 8 Foreshortening formulation vs. ANCF in the first example

Table 1 CPU-times for all the formulations in the 2D spin-up beam

Formulation	FNL1	FNL2	FS0
Time (s)	0.281	0.297	0.250
Δy (mm)	28.295	6.486	2.614

4.2 Three-dimensional case

In this example, a gravity acceleration of 9.81 m/s^2 is added to the problem, in the negative direction of the z axis, leading to a three-dimensional problem. One static and two dynamic transversal modes are added in the z direction to capture vertical deflections, making a total of six modes, plus the eventually needed axial ones in the FNL method. Before starting the simulation, the beam is let to reach its equilibrium position.

The extension of both the FNL and FS methods to the three-dimensional case is straightforward, since the effects in y and z directions can be considered independent. In the FNL formulation, there are no substantial changes, and in the FS case, the foreshortening can be obtained from the following expression, where w_0 is the neutral axis displacement in the z direction [6, 7],

$$u_{fs}(x) = -\frac{1}{2}\int_{x_0}^{x} \left(v_0'^2 + w_0'^2\right) \mathrm{d}x \tag{40}$$

Only the first nonlinear and the foreshortening methods are addressed in this example, and since the results in the y direction are approximately the same as obtained in the plane case, only the displacements in x and z directions are now shown and discussed. These results are compared to a reference solution obtained with a nonlinear finite element model, discretized into 20 elements and with the same integration parameters. In order to obtain a numerical value for the error, the position of the beam tip (in the local frame) is compared to that of the reference solution. For the x direction,

$$\Delta x = \frac{1}{ns+1}\sum_{i=0}^{ns} \left| x_i - x_i^* \right| \tag{41}$$

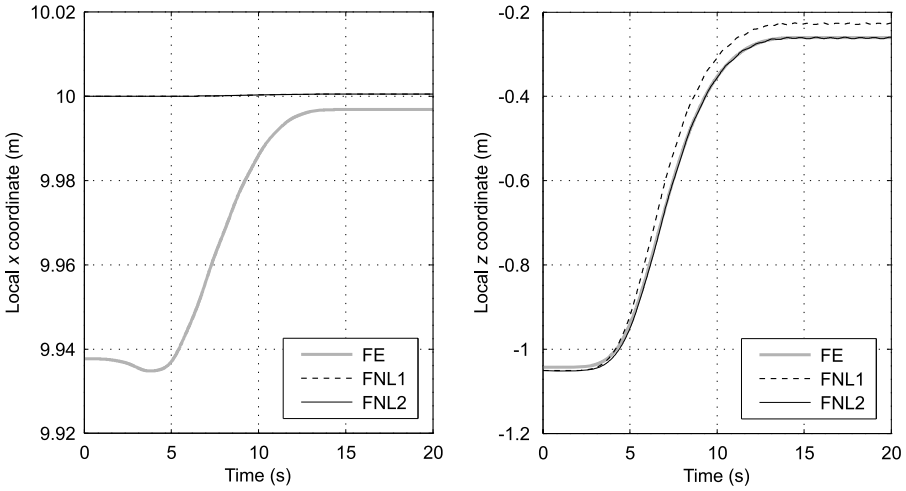

Fig. 9 First nonlinear formulation vs. FE in the second example

where x_i and x_i^* are the calculated and reference values respectively, and ns is the number of time-steps. The same may be done for y and z directions.

The first nonlinear formulation, whose results are shown in Fig. 9, does not obtain acceptable results for the axial displacement, no matter how many axial modes are introduced. This happens because the $\mathbf{K}_G$ elements corresponding to axial modes are equal to zero, thus introducing no modification in their associated stiffnesses. At the equilibrium position, there is a tip displacement of more than 6 cm in the z direction, which is not captured, and the error at the steady-state stage is about 3.5 mm with respect to the reference. This is because the large deflection makes the foreshortening effect much more relevant than the actual beam shortening. As it happened in the y direction, the beam with only one axial mode (FNL1) is excessively rigidized, needing an extra mode (FNL2) to obtain reasonably accurate results.

In the case of the foreshortening method, as can be seen in Fig. 10, the precision in the x direction is significantly improved. The steady-state error is around 0.5 mm with no axial modes, lowering to 0.01 mm if one axial mode is added. In the vertical direction, the results are approximately the same obtained with the FNL2 formulation, despite using only bending modes.

In Table 2, the CPU-times and deviations from the reference solution are shown for all the formulations. The FS values are shown for none, one, and two axial modes, although Fig. 10 represents the results for the first case. It can be seen that the FNL formulation is faster for the same number of modes, but when the efficiency is compared for a similar level of accuracy in y and z directions, the FS method is slightly faster (i.e., FNL2 vs. FS0).

5 Conclusion

The implementation of two techniques for accounting for the foreshortening effect into a FFR formulation in natural coordinates has been presented. Both of them are easy to implement, and obtain very good performance if compared to ANCF or nonlinear FEM.

As it has been shown in the tests, the linear formulation yields incorrect results, which means that any of the higher order formulations must be used. The first nonlinear formula-

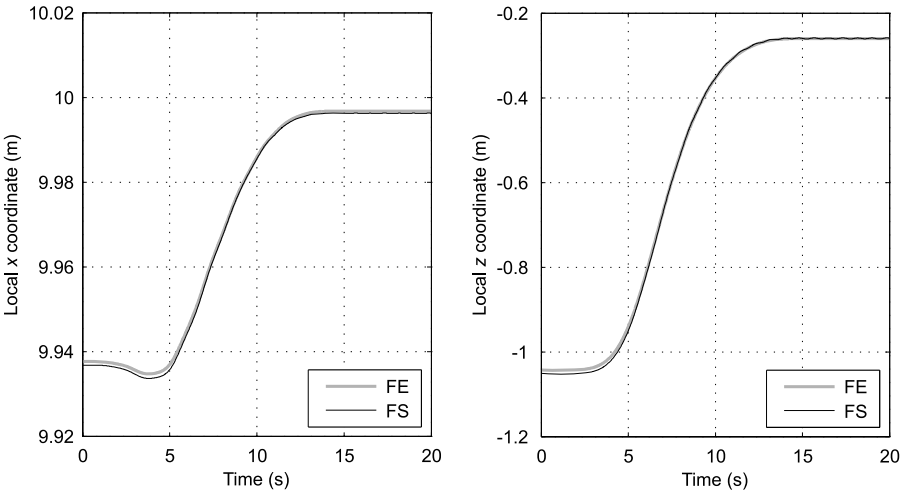

Fig. 10 Foreshortening formulation vs. FE in the second example

Table 2 CPU-times for all the formulations in the 3D spin-up beam

Formulation	FNL1	FNL2	FS0	FS1	FS2
Time (s)	0.328	0.359	0.336	0.367	0.399
Δx (mm)	27.921	27.921	0.647	0.387	0.387
Δy (mm)	28.295	6.486	2.614	2.612	2.611
Δz (mm)	32.066	4.119	3.462	3.464	3.465

tion is very easy to implement, but presents some problems, since only one axial mode is not sufficient for obtaining accurate results, and the use of axial modes of high natural frequencies hinders the integration process. If the deflections are large enough, this method fails also to accurately measure the x displacements. The foreshortening formulation has proven to be the fastest and also the most accurate. It does not require axial modes for obtaining good results for the transversal deflections and, in case that axial stresses are needed, longitudinal modes can be added without problems. For the same number of modes, it is slightly slower since it involves more operations, but if the efficiency/accuracy ratio is considered, it is always advantageous to include the foreshortening in the kinematic modeling.

Acknowledgements This research has been sponsored by the Spanish MEC (Grant No. DPI2006-15613-C03-01) and the Galician DGID (Grant No. PGIDT04PXIC16601PN).

References

1. Shabana, A.A.: Dynamics of Multibody Systems, 3rd edn. Cambridge University Press, Cambridge (2005)
2. Kane, T.R., Ryan, R.R., Banerjee, A.K.: Dynamics of a cantilever beam attached to a moving base. AIAA J. **10**(2), 131–151 (1987)
3. Mayo, J., Domínguez, J., Shabana, A.A.: Geometrically nonlinear formulations of beams in flexible multibody dynamics. J. Vib. Acoust. **117**, 501–509 (1995)

4. Mayo, J., García, D., Domínguez, J.: Study of the geometric stiffening effect: comparison of different formulations. Multibody Syst. Dyn. **11**(4), 321–341 (2004)
5. Sharf, I.: Geometrically non-linear beam element for dynamics simulation of multibody systems. Int. J. Numer. Methods Eng. **39**, 763–786 (1996)
6. Shi, P., McPhee, J., Heppler, G.R.: A deformation field for Euler–Bernoulli beams with applications to flexible multibody dynamics. Multibody Syst. Dyn. **5**(1), 79–104 (2001)
7. Valembois, R.E., Fisette, P., Samin, J.C.: Comparison of various techniques for modelling flexible beams in multibody dynamics. Nonlinear Dyn. **12**(4), 367–397 (1997)
8. Bathe, K.J.: Finite Element Procedures. Prentice Hall, Englewood Cliffs (1995)
9. García de Jalón, J., Bayo, E.: Kinematic and Dynamic Simulation of Multibody Systems. Springer, Berlin (1994)
10. Cuadrado, J., Gutiérrez, R., Naya, M.A., González, M.: Experimental validation of a flexible MBS dynamic formulation through comparison between measured and calculated stresses on a prototype car. Multibody Syst. Dyn. **11**(2), 147–166 (2004)
11. Newmark, N.M.: A method of computation for structural dynamics. J. Eng. Mech. Div. ASCE **85**(EM3), 67–94 (1959)
12. Craig, R.R., Bampton, M.C.C.: Coupling of substructures for dynamic analyses. AIAA J. **6**(7), 1313–1319 (1968)
13. Géradin, M., Cardona, A.: Flexible Multibody Dynamics: A Finite Element Approach. Wiley, New York (2001)
14. Omar, M.A., Shabana, A.A.: A two-dimensional shear deformable beam for large rotation and deformation problems. J. Sound Vib. **243**, 565–576 (2001)